# Aerosol retrieval and atmospheric correction of HJ-1 CCD data over Beijing

**FANG Li[1], YU Tao[1], GU Xingfa[1], WANG Shupeng[1], GAO Jun[2], LIU Qiyue[1]**

1. *State Key Laboratory of Remote Sensing Science, Jointly Sponsored by the Institute of Remote Sensing and Digital Earth, Chinese Academy of Sciences and Beijing Normal University, Beijing* 100101, *China*
2. *Administration on Science, Technology, and Industry for National Defense, Beijing* 100037, *China*

**Abstract:** Compared to moderate/low resolution satellite sensors for aerosol detection, the high spatial resolution of HJ-1 CCD camera (30 m) provides an opportunity to easily find spectrally pure pixels (SPP) over urban areas. In this study, we developed an SPP algorithm for urban Aerosol Optical Depth (AOD) retrieval using HJ-1 CCD data. Pixel Purity Index (PPI) is used to identify the pure pixels in the image. The surface reflectances of the pure pixels were estimated from the multi-temporal CCD measurements of HJ-1A and HJ-1B based on the surface Bi-directional Reflectance Distribution Function (BRDF) model. Then the AOD can be retrieved from satellite measurements. The comparison with ground-based AErosol RObotic NETwork AERONET AOD measurements shows good performance of our algorithm. A significant correlation coefficient with $R$=0.83 was obtained with a linear regression slope close to 1 and a intercept of 0.053. With the retrieved AOD as an input, HJ-1CCD data over urban areas was significantly improved after the atmospheric correction.

**Key words:** aerosol optical depth, aerosol retrieval, HJ-1 CCD, atmospheric correction, pure pixel

**CLC number:** TP79/P407.4 **Document code:** A

**Citation format:** **Fang L, Yu T, Gu X F, Wang S P, Gao J, Liu Q Y. 2013. Aerosol retrieval and atmospheric correction of HJ-1 CCD data over Beijing. Journal of Remote Sensing, 17(1): 151–164**

## 1 INTRODUCTION

Accurate radiative calibration of airborne or spaceborne sensors and the atmospheric correction of remote sensing data are the basis of quantitative remote sensing (Kaufman & Sendra, 1988). The radiation measured by the satellite sensor is the coupling of signals contributed by the surface and the atmosphere. The perturbation of atmosphere may lead to indistinctness and decline in contrast of the satellite image, as well as the lost of details. Moreover, it may affect the subsequent quantitative retrievals such as surface reflectance, vegetation index, and chlorophyll concentration, causing significant deviation from the true values of these parameters. Accurate atmospheric correction of satellite data significantly depends on the input atmospheric parameters, among which aerosol properties have the greatest influence (Fallah, et al., 1997; Liang, et al., 2001). Aerosol optical depth (AOD) and the aerosol models used in the atmospheric correction remarkably influence the surface reflectance, therefore accurate determination of aerosol optical properties and its spatial and temporal distributions become the essential part in the quantitative applications of remote sensing.

Remote sensing technique is increasingly used to obtain the global information on aerosol properties due to its high coverage and low cost (Kokhanovsky & Leeuw, 2009), it includes using multi-spectral information (Kaufman, et al., 1997; Levy, et al., 2007), multi-angular information (Peter & North, 2002; Diner, et al., 2005), and multi-angular polarization information (Waquet, et al., 2007; Tanré, et al., 2011). Since late 1999, Moderate-Resolution Imaging Spectro radiometer (MODIS) has been widely used for aerosol retrieval over China (Li, et al., 2007; Xie, et al., 2011). Retrieval of aerosol optical properties (aerosol optical depth and Fine Model Weighting at 0.55 μm) is achieved using the dark dense vegetation (DDV) method. The Collection 005 (C5) version of the algorithm introduced more accurate aerosol models and surface reflectance relationship between the visible bands (470 nm and 660 nm) and the 2130 nm in 2007. The new algorithm performance is largely improved as compared to the previous Collection 004(C4) algorithm over China. However, the C5 AOD products show less agreement with ground-based measurements over some urban areas (Li, et al., 2007; Xie, et al., 2011), which can probably be attributed to the uncertainty in the surface reflectance relationship for urban complex underlying surface (Oo, et al.,2010).

Most currently operational satellite sensors for aerosol detection have low-moderate spatial resolution, such as MODIS, Multi-angle Imaging Spectro-Radiometer (MISR) and Polarization and Directionality of the Earth Reflectance (POLDER). Over urban areas,

**Received:** 2011-12-26; **Accepted:** 2012-03-12
**Foundation:** National Basic Research Program (973 Program) (No. 2010CB950803)
**First author biography:** FANG Li (1985— ), female, Ph.D. candidate, her research interest is atmospheric remote sensing. E-mail: lifang@irsa.ac.cn
**Corresponding author biography:** YU Tao (1967— ), male, professor, his research interest is quantitative remote sensing. E-mail: yutao@irsa.ac.cn

the imaging pixels of such sensors are usually mixed pixels including several surface types. A significant influence factor for aerosol retrieval over urban areas lies in the uncertainty in the estimated surface reflectances of the mixed pixels, which is hard to characterize accurately due to the complex surface types. Therefore, accurate retrieval of aerosol properties over complex underlying surface remains a challenge of remote sensing of aerosols. Compared to mixed pixels, the spectrally pure pixels (SPP) are dominated by only one typical surface type, whose spectrum is the end-member of mixed pixels. The surface reflectances of pure pixels are relatively more stable and easier to characterize by ground-based measurements or surface reflectance model. Thus aerosol retrieval for pure pixels may become a new approach for accurate retrieval of aerosol properties over complex underlying surface.

Compared to the currently operational satellite sensors for aerosol detection, the high spatial resolution of HJ-1 CCD camera (30 m) provides an opportunity to easily find spectrally pure pixels over urban areas. In this study, an SPP algorithm is developed for retrieving aerosol optical depth (AOD) over urban areas from HJ-1 CCD observations, taking advantage of the high spatial resolution of the CCD cameras. The derived AODs are used to improve the accuracy of atmospheric correction of the CCD image.

## 2 THE SPP AEROSOL RETRIEVAL ALGORITHM OVER URBAN AREAS

### 2.1 Basic strategy

Assuming that the atmosphere is horizontally uniform and vertically non-uniform, the measured reflectance at the top of the atmosphere is a function of successive orders of radiation interactions in the coupled surface atmosphere system. The top of atmosphere (TOA) angular spectral reflectance at a wavelength $\lambda$ results from the following: Scattering of radiation within the atmosphere without interaction with the surface (known as the 'atmospheric path reflectance'), the reflection of radiation off the surface that is directly transmitted to the TOA (the 'surface function'), and the reflection of radiation from outside the sensor's field of view (the 'environment function'). So the TOA angular spectral reflectance can be approximated as (Vermote, et al., 1997; Levy, et al., 2007)

$$\rho_\lambda^*(\theta_0,\theta,\phi)=\rho_\lambda^{\mathrm{a}}(\theta_0,\theta,\phi)+\frac{\rho_\lambda^{\mathrm{s}}}{1-\rho_\lambda^{\mathrm{s}}\cdot S_\lambda}\cdot T_\lambda(\theta_0)\cdot T_\lambda(\theta) \tag{1}$$

where $\theta_0$, $\theta$, $\phi$ are solar zenith, view zenith and relative azimuth angles respectively; $\rho_\lambda^{\mathrm{a}}$ is the atmospheric 'path reflectance'; $T_\lambda(\theta_0)$ and $T_\lambda(\theta)$ are the downward and upward atmospheric transmissions; $S_\lambda$, is the atmospheric spherical albedo, and $\rho_\lambda^{\mathrm{s}}$ is the bidirectional spectral surface reflectance. On the right side of Eq. (1), $\rho_\lambda^{\mathrm{a}}$, $S_\lambda$, and $T_\lambda(\theta_0)\cdot T_\lambda(\theta)$ are functions of the aerosol optical depth ($\tau$). Remote sensing of aerosol stems from these three atmospheric parameters (take $T_\lambda(\theta_0)\cdot T_\lambda(\theta)$ as one parameter).

### 2.2 Identification of the spectrally pure pixels

In this study, the Pixel Purity Index (PPI) is used to identify the pure pixels within the CCD image (Boardman, et al., 1993). PPI has been successfully used as a method to find the pixels with the "purest spectrum" from Hyperspectral satellite data. The spectral radiation measured by satellite sensors is nonnegative; vectors composed of the discrete spectrum form a convex *multidimensional* region in the *multidimensional* space. Boundary of the convex *multidimensional* region corresponds to pure pixels whose spectrum is the end-member of mixed pixels, while other vectors inside the convex *multidimensional* region is considered to be linearly combined by the boundary-vectors. Specifically, the N-dimensional scattered plots are projected repeatedly onto separate random vectors. The pixels correspond to extremes of each projection are identified and accumulatively counted, resulting in a pixel purity index image whose value of each pixel being the number of times counted during the process of repeated projection. Pure pixels are those have higher values within the pixel purity index image (Boardman, et al., 1993). The PPI method has also been successfully applied to multispectral satellite images (Hu, et al., 2010).

### 2.3 Introduction of the new algorithm

Another advantage of the HJ-1 CDD camera is its multi-temporal observation capability, particularly when we combine observations from both HJ-1A and HJ-1B platforms. This advantage enables us to collect a set of observations with different imaging directions for the same pixel during a temporal window, which includes both "clear" day images and "hazy" day images. For aerosol retrieval over bright underlying surfaces, such as arid or semi-arid areas (deserts) and urban areas, several algorithms have been developed to derive the AOD of hazy days with the surface reflectances obtained from the clear day images, assuming that the surface reflection property is relatively stable within this temporal window. These algorithms include the deep blue algorithm (Hsu, et al., 2004), the contrast reduction algorithm (Tanré, et al., 1988) and the improved algorithm for retrieving aerosol optical depth from MODIS imagery over bright surfaces (Liang, et al., 2006). The length of the temporal window is set to be a three-month period in the study of Liang, et al. (2006), however, one-month period (Hsu, et al., 2004) is considered to be better if adequate clear observations were included. However, the assumption may introduce large uncertainty when applied to mixed pixels in urban areas. Surface reflection of the mixed pixels in urban areas tends to be easily affected by human activities; on the other hand, with the variation of imaging geometries, the shadowing caused by high buildings in urban areas make it more difficult to determine the surface reflectances of the mixed pixels. In this study, most of the selected stable pure pixels using PPI method are located in the center of large uniform surface target, which are possibly less affected by human activities and the building-shadowing. Furthermore, using pure pixels may reduce the uncertainty in characterizing the reflection of mixed pixels using surface BRDF model.

The main procedures to derive aerosol optical depth using HJ-1 CCD data are discussed as below.

(1) Pre-calculating the look-up tables (LUT). The atmospheric optical properties (i.e. path reflectance and atmospheric transmissions) are pre-calculated for several aerosol loadings using 6S radiative transfer codes (Vermote, et al., 1997) based on analysis of the regional aerosol model.

(2) Calculating the apparent reflectance measured by the CCD camera using absolute calibration coefficients and the cloud discrimination after cloud detection.

(3) Selecting several clear days images within the temporal window and the identification of the spectrally pure pixels using PPI method. Since the surface property in urban areas is significantly influenced by human activities, the pure pixels identified from different clear images may vary slightly, thus only those stably obtained from all clear images are finally kept for retrieving aerosol optical depth.

(4) Determining the surface BRDF of the pure pixels from the clear observations with a BRDF model. Then the surface reflectances of the haze observations are interpolated from the fitted surface BRDF using the corresponding imaging geometries. The Roujean BRDF model (Roujean, et al., 1992) is used in this study which requires at least three observations to determine the model parameters for a certain pixel, thus at least three clear images should be selected in Step (3). For each pure pixel, the parameters required to characterize the BRDF model are derived from the multiple directional surface reflectances, which are converted from the measured TOA radiance through atmospheric correction of the clear images. With the obtained model parameters as well as the imaging geometries, the directional surface reflectances of the pure pixels of the hazy observations are interpolated from the surface temporal BRDF.

(5) Retrieving aerosol optical depth of the pure pixels for the hazy days based on the LUT. The spatial variation of aerosol optical depth is much smoother than the surface features (Liang, et al., 2006). Under the condition that pure pixels are well-distributed, linear interpolation is finally performed to obtain the aerosol optical depth of the whole image.

## 2.4 Validation and analysis

The previous studies (Wang, et al., 2011) show that aerosol model of Beijing is composed of mixtures of fine and coarse particles with the domination of fine urban pollutants. However, the spring season is more influenced by coarse dust particles. The monthly mean AOD over Beijing ranges between 0.5 and 1.8. During the period from August to October, 2009, the coarse-fine particles volume ratio averaged from Aerosol Robotic Network (AERONET) (Holben, et al., 1998) measurements at Beijing site is 1.37. To examine the performance of our algorithm, we performed AOD retrievals over Beijing from the HJ-1 CCD observations from August to October, 2009. The retrieval results were validated by the ground-based measurements from a sun photometer (CE318) at the AERONET Beijing site. The MODIS aerosol products close to the HJ-1 pass time were also evaluated using AERONET measurements. All the satellite retrievals and ground measurements were calculated at 550 nm to guarantee the consistency of the data.

Based on the AERONET AOD measurements nearest to HJ-1 overpass time, the days with AOD at 500 nm less than 0.10 is considered as the “clear” atmospheric condition at Beijing, while the mean AOD calculated from AERONET measurements between 2005 and 2009 is 0.86. Fig. 1 shows the location of AERONET Beijing site (39.977°N, 116.381°E) on the true color composite CCD image using the red, green, and blue bands. The identified pure pixels around the AERONET site are also shown in the image.

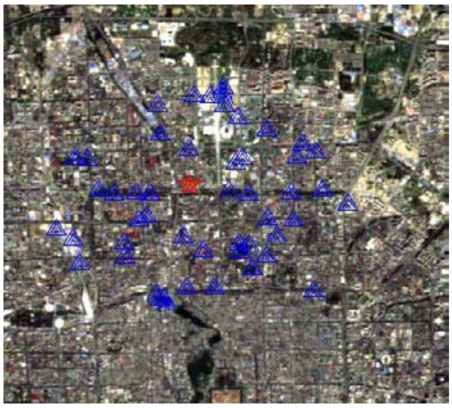

Fig. 1 Location of AERONET Beijing site (red star) and distribution of the surrounding pure pixels (blue triangles)

A constant atmospheric visibility, i.e. 100 km, was used to perform atmospheric correction of the clear images. Fig. 2 demonstrates the resulting BRDF for two typical surface types (cement road: 40.000°N, 116.382°E; grass: 39.974°N, 116.391°E) at the blue band.

The comparison of AOD retrieved from HJ-1 CCD observations with the sunphotometer measurements of AERONET is shown in Fig. 3. We used AERONET Level 2 quality assured data nearest to the HJ-1 overpass time for comparison. The time intervals between AERONET measurements and satellite overpasses were within 0.5 h for all the match-ups to ensure stable atmospheric conditions. Fig. 3 indicates good agreement between the retrieved AOD using our algorithm and the ground measurements with a high correlation of 0.83. The linear regression slope and intercept are 1.091 and 0.053, respectively. And the Root-Mean-Square Error(RMSE)is 0.15.

Fig. 3 also shows the validation of MODIS aerosol products close to the HJ-1 pass time against AERONET measurements. The time intervals between MODIS and HJ-1 overpasses were within 0.5 h for all the coincidences except for that of October 15$^{th}$, 2009, which was approximately 35 min. The caption in the plot reports the correlation coefficient, the linear regression slope and intercept, which are 1.216, 0.183 and 0.87, respectively. The RMSE is 0.27. Fig. 3 suggests that the slope, intercept as well as the RSME corresponding to HJ-1 AODs are superior to those of MODIS. However, the correlation is slightly lower. Table 1 lists the HJ-1 AOD retrievals, MODIS AOD products, and the AERONET measurements of all the coincidences. The relative differences of satellite retrievals with AERONET AODs are also listed in Table 1. It can be seen that the relative differences of HJ-1 AODs are generally lower than those of MODIS AODs. The average difference is 49% and 139% for HJ-1 and MODIS, respectively. Both HJ-1 and MODIS retrievals have several coincidences with relative difference beyond $0.05+0.15\times\tau_{\mathrm{AERONET}}$, which is the criterion used to define an accurate AOD retrieval over land (Remer, et al., 2005). One possible reason is that it is still difficult to accurately determine

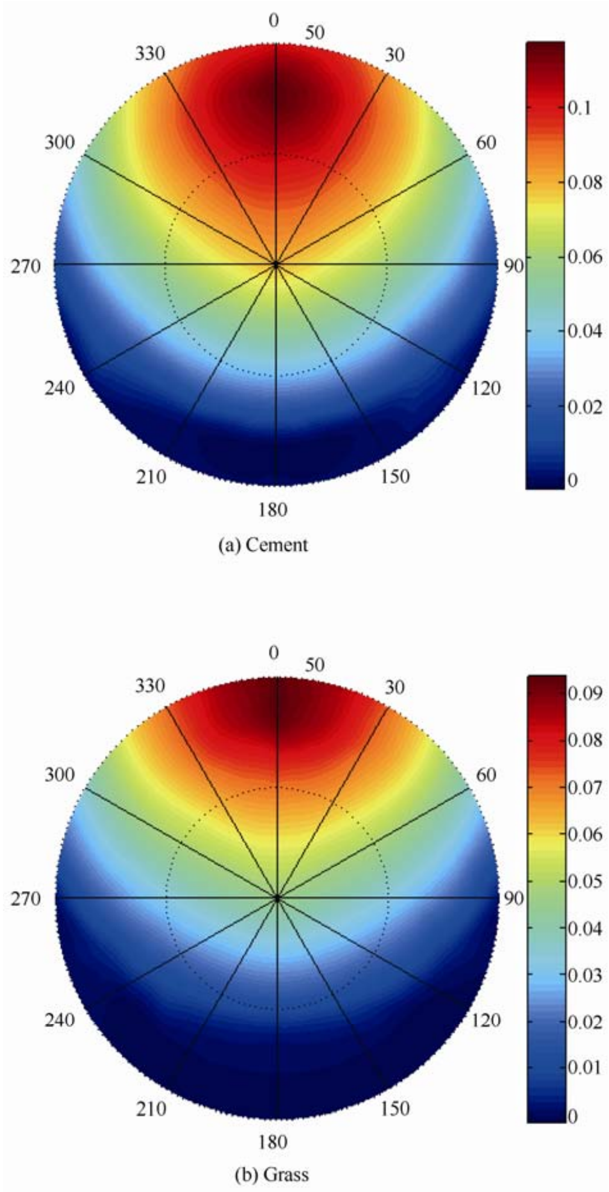


Fig. 2 The simulated BRDF at the blue band for cement road and grass

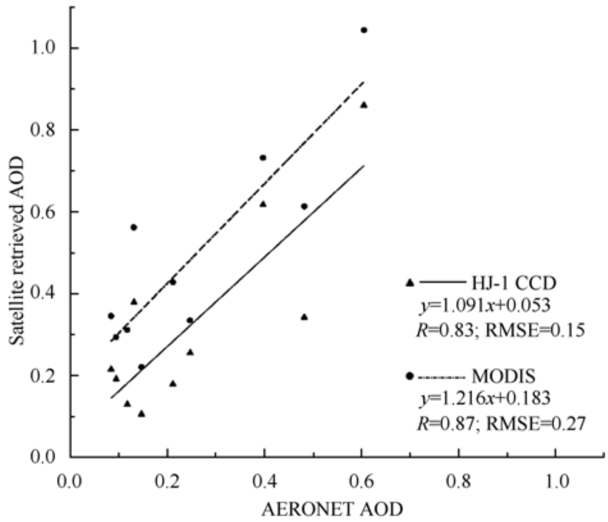


Fig. 3 Validation of HJ-1 CCD AOD and MODIS AOD against AERONET AOD measurements

the urban surface reflectance due to heterogeneity, though pure pixels are used. Another possible reason lies in the low AOD values of the validation samples (the average AOD is 0.25). In the atmosphere-Earth surface system illuminated by the sun, the lower contribution of atmosphere leads to lower sensitivity of the satellite measured radiation to aerosol optical properties (Bréon, et al., 2011). However, generally, the SPP method can be effectively used to monitor urban aerosols and to further provide the parameters for atmospheric correction of HJ-1 CCD data.

## 3 ATMOSPHERIC CORRECTION OF HJ-1 CCD IMAGE BASED ON RADIATIVE TRANSFER MODEL

Based on the retrieved AOD using SPP method, we performed atmospheric correction of HJ-1 CCD image to obtain the surface directional reflectance of each pixel, which is realized through the pre-established LUT containing atmospheric parameters. Fig. 4 and Fig.5 show the TOA and atmospheric corrected reflectance image covering Beijing on August 13$^{rd}$, 2009 for the blue band and red band, respectively.

**Table 1 AODs of HJ-1 CCD, MODIS, AERONET and the relative error against AERONET AODs**

| Date | HJ-1 AOD | MODIS AOD | AERONET AOD | Relative error of HJ-1 AOD/% | Relative error of MODIS AOD/% |
|---|---|---|---|---|---|
| 2009-08-02 | 0.3792 | 0.5620 | 0.1311 | 189 | 329 |
| 2009-08-13 | 0.6172 | 0.7320 | 0.3969 | 56 | 84 |
| 2009-08-23 | 0.3426 | 0.6130 | 0.4817 | –29 | 27 |
| 2009-09-21 | 0.1300 | 0.3120 | 0.1175 | 11 | 166 |
| 2009-10-02 | 0.2153 | 0.3460 | 0.0842 | 156 | 311 |
| 2009-10-05 | 0.1794 | 0.4280 | 0.2113 | –15 | 103 |
| 2009-10-09 | 0.8600 | 1.0440 | 0.6044 | 42 | 73 |
| 2009-10-14 | 0.1920 | 0.2940 | 0.0945 | 103 | 211 |
| 2009-10-15 | 0.2559 | 0.3350 | 0.2468 | 4 | 36 |
| 2009-10-17 | 0.1061 | 0.2210 | 0.1467 | –28 | 51 |
| **Average** | **0.3278** | **0.4887** | **0.2515** | **49** | **139** |

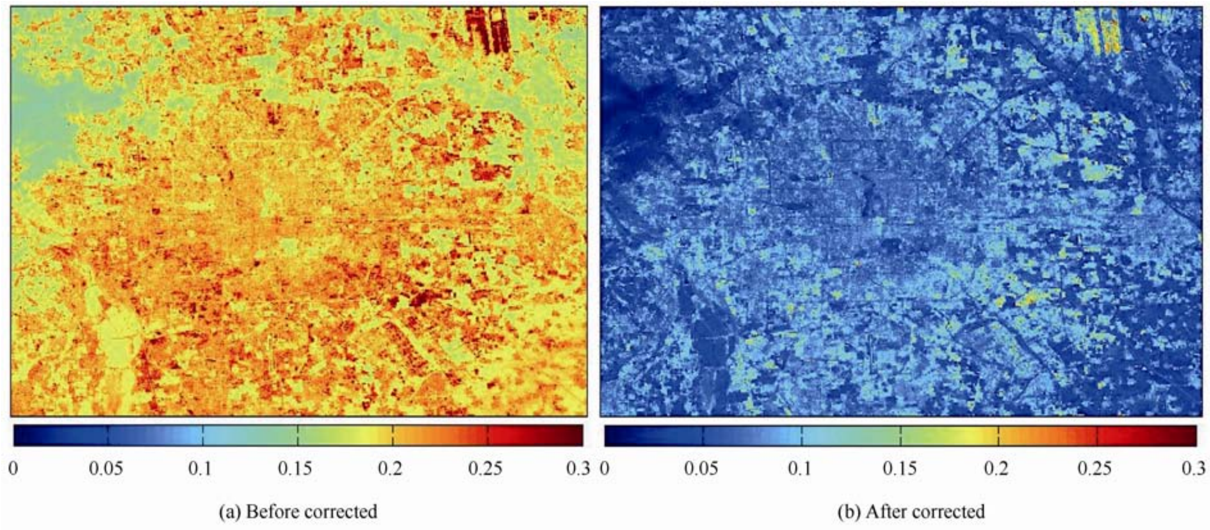


Fig. 4 The TOA and atmospheric corrected reflectance images at the blue band

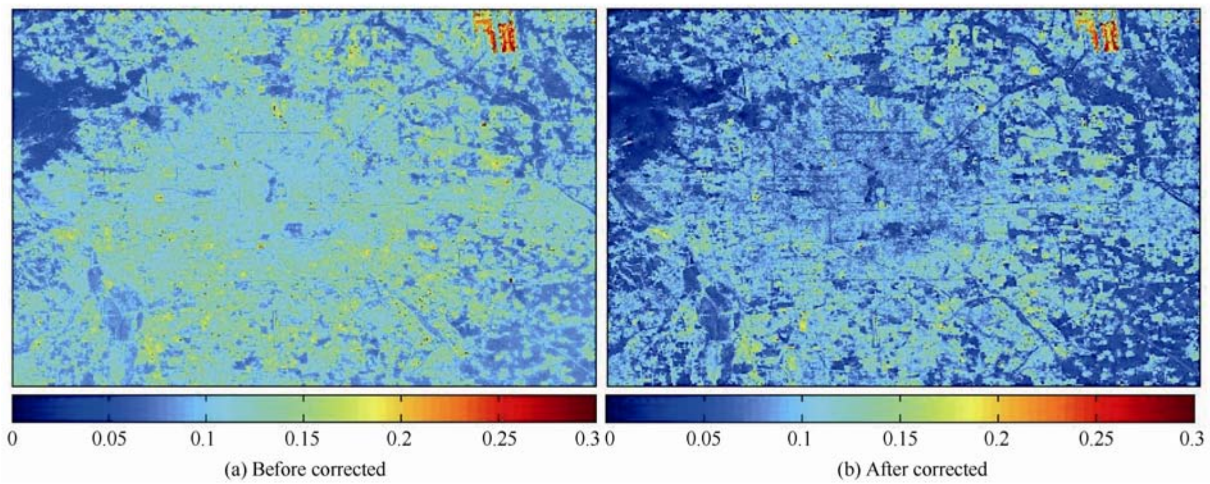


Fig. 5 The TOA and atmospheric corrected reflectance images at the red band

Obvious discrepancy in reflected radiance and image contrast is found between the TOA and atmospheric corrected images. The satellite observed surface is affected by atmospheric scattering and gaseous absorptions leading to image blurring and low image contrast. However, the influences of aerosol scattering and gaseous absorption by water vapor and ozone are largely eliminated after atmospheric correction. Higher image definition and contrast is achieved. As molecular scattering and aerosol scattering have higher influence at shortwave band, it can be found from Fig. 4 and Fig.5 that the variations between the TOA and atmospheric corrected images at the blue band are greater than those of the red band.

To quantitatively evaluate the accuracy of atmospheric correction for HJ-1 CCD data, the surface reflectances before and after atmospheric correction were compared with the ground-based measured surface reflectances. The atmospheric corrected results for HJ-1 CCD data using image-based DOS (dark object subtraction) method (Kaufman, 1989) were also included in the comparison. Fig. 6 demonstrates the location of the validation sites (cement road: 39.993$^{o}$N, 116.393$^{o}$E; grass: 39.991$^{o}$N, 116.434$^{o}$E) on the CCD image acquired on August 13$^{rd}$, 2009. And the comparison among the independently obtained surface reflectances is shown in Fig.7.

It indicates significant variations between the TOA and corrected reflectance, where the latter shows higher agreement with the ground data. The influence caused by atmospheric scattering and absorption is effectively corrected. Compared to the image-based DOS method, our method gives results more close to the ground data, indicating significant improvement in correction accuracy.

Fig. 6 Location of the ground sites used for validation of atmospheric correction (Red: cement road; Green: grass)

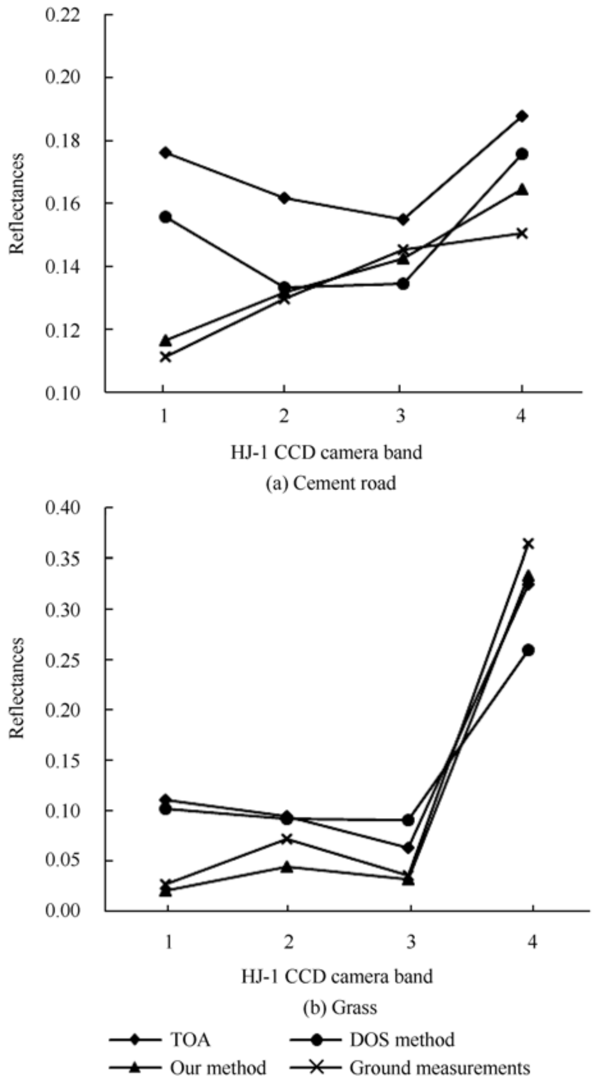


Fig. 7 The TOA, atmospheric corrected, and ground-based measured spectral reflectances for cement road and grass

## 4 CONCLUSIONS

In this study a SPP algorithm was developed for retrieving aerosol optical depth from HJ-1 CCD observations over urban areas. The retrieval results are validated by the ground-based measurements from a sun photometer (CE318) at the AERONET Beijing site. The comparison indicates good agreement between the retrievals using our algorithm and the ground-based measurements with a high correlation of 0.83. The linear regression slope and intercept are 1.091 and 0.053, respectively. And the RMSE is 0.15. The MODIS aerosol products close to the HJ-1 pass time were also evaluated using AERONET measurements. The intercomparison with MODIS preliminarily indicates the algorithm is promising for AOD retrieval over urban areas. Based on the retrieved AOD, atmospheric correction is performed for HJ-1 CCD observations over Beijing. Both the visual contrast between TOA and corrected image and the quantitative validation against ground-based measured reflectances demonstrate good performance of the atmospheric correction, which would promote the quantitative application of HJ-1 data. However, more validation work is required to evaluate the robustness and accuracy of the aerosol retrieval algorithm.

## REFERENCES

Boardman J W, Kruse F A and Green R O. 1993. Automating spectral unmixing of AV I R IS data using convex geometry concepts // Summaries, Forth Annual JPL Airborne Geoscience Workshop. Pasadena, CA, US: JPL Publication, 26(1): 11−14

Bréon F M, Vermeulen A and Descloitres J. 2011. An evaluation of satellite aerosol products against sunphotometer measurements. Remote Sensing Environment, 115(12): 3102−3111 [DOI: 10.1016/j.rse.2011.06.017]

Diner D J, Martonchik J V, Kahn R A, Pinty B, Gobron N, Nelson D L and Holben B N. 2005. Using angular and spectral shape similarity constraints to improve MISR aerosol and surface retrievals over land. Remote Sensing of Environment, 94(2): 155−171

Fallah A, Jaja J, Liang S, Kaufman Y J and Townshend J R G. 1997. Fast algorithms for atmospheric correction from Landsat TM over land. Journal of Geophysical Research, 102: 17173−17186

Holben B N, Eck T F, Slutsker I, Tanré D, Buis J P, Setzer A, Vermote E, Reagan J A, Kaufman Y J, Nakajima T, Lavenu F, Jankowlak I and Smirnov A. 1998. AERONET-A federated instrument network and data archive for aerosol characterization. Remote Sensing of Environment, 66(1): 1−16 [DOI: 10.1016/S0034-4257(98)00031-5]

Hsu N C, Tsay S C, King M D and Herman J R. 2004. Aerosol properties over bright-reflecting source regions. IEEE Transacitons on Geoscience and Remote Sensing, 42(3): 557−569 [DOI: 10.1109/TGRS.2004.824067]

Hu S J, Hu D Y and Zhao W J. 2010. Extract urban vegetation coverage based on LSMM and improved FCM: a case study in Haidian District. Acta Ecologica Sinica, 30(4): 1018−1024

Kaufman Y J. 1989. The atmospheric effect on remote sensing and its correction // Asrar G, ed. Theory and Application of Optical Remote Sensing, New York: Wiley: 341

Kaufman Y J and Sendra C. 1988. Algorithm for automatic atmospheric corrections to visible and near-IR satellite imagery. International Journal of Remote Sensing, 9(8): 1357−1381 [DOI: 10.1080/01431168808954942]

Kaufman Y J, Tanré D, Remer L A, Vermote E F, Chu A and Holben B N. 1997. Operational remote sensing of tropospheric aerosol over land from EOS moderate resolution imaging spectroradiometer. Journal of Geophysical Research, 102(D14): 17051−17067 [DOI: 10.1029/96JD03988]

Kokhanovsky A A and Leeuw G. 2009. Satellite Aerosol Remote Sensing Over Land. UK: Praxis Publishing Ltd, Chichester

Levy R C, Remer L A, Mattoo S, Vermote E F and Kaufman Y J. 2007. Second-generation operational algorithm: retrieval of aerosol properties over land from inversion of Moderate Resolution Imaging Spectroradiometer spectral reflectance. Journal of Geophysical Research, 112: D13211 [DOI: 10.1029/ 2006JD007811]

Li Z Q, Niu F, Lee K H, Xin J Y, Hao W M, Nordgren B L, Wang Y S and Wang P C. 2007. Validation and understanding of Moderate Resolution Imaging Spectroradiometer aerosol products (C5) using ground-based measurements from the handheld Sun photometer network in China. Journal of Geophysical Research, 112:

D22S07 [DOI: 10.1029/2007JD008479]

Liang S, Fang H and Chen M. 2001. Atmospheric correction of landsat ETM+ land surface imagery: I. Methods. IEEE Transactions on Geoscience and Remote Sensing, 39(11): 2490−2498 [DOI: 10.1109/36.964986]

Liang S L, Zhong B and Fang H L. 2006. Improved estimation of aerosol optical depth from MODIS imagery over land surfaces. Remote Sensing of Environment, 104(4): 416−425 [DOI: 10.1016/j.rse.2006.05.016]

Oo M M, Jerg M, Hernandez E, Picon A, Gross B M, Moshary F and Ahmed S A. 2010. Improved MODIS aerosol retrieval using modified VIS/SWIR surface albedo ratio over Urban Scenes. IEEE Transactions on Geoscience and Remote Sensing, 48(3): 983−1000 [DOI: 10.1109/TGRS.2009.2028333]

Peter R and North J. 2002. Estimation of aerosol opacity and land surface bidirectional reflectance from ATSR-2 dual-angle imagery: operational method and validation. Journal of Geophysical Research (Atmos), 107: 4149 [DOI: 10.1029/ 2000JD0-00207]

Remer L A, Kaufman Y J, Tanré D, Mattoo S, Chu D A, Martins J V, Li R R, Ichoku C, Levy R C, Kleidman R G, Eck T F, Vermote E, and Holben B N. 2005. The MODIS Aerosol algorithm, products, and validation. Journal of the Atmospheric Sciences, 62(4), 947−973 [doi: 10.1175/JAS3385.1]

Roujean J L, Leroy M and Deschamps P Y. 1992. A bidirectional reflectance model of the Earth’s surface for the correction of remote sensing data. Journal of Geophysical Research, 97(D18): 20455−20468 [DOI: 10.1029/92JD01411]

Tanré D, Bréon F M, Deuzé J L, Dubovik O, Ducos F, Francois P, Goloub P, Herman M, Lifermann A and Waquet F. 2011. Remote sensing of aerosols by using polarized, directional and spectral measurements within the A-Train: the PARASOL mission. Atmospheric Measurement Techniques Discussions, 4(2): 2037−2069 [DOI: 10.5194/amtd-4-2037-2011]

Tanré D, Deschamps P Y, Devaux C and Herman M. 1988. Estimation of Saharan aerosol optical thickness from blurring effects in thematic mapper data. Journal of Geophysical Research, 93(D12): 15955−15964 [DOI: 10.1029/JD093iD12p15955]

Vermote E F, Tanré D, Deuzé J L, Herman M and Morcette J J. 1997. Second simulation of the satellite signal in the solar spectrum, 6S: an overview. IEEE Transactions on Geoscience and Remote Sensing, 35(3): 675−686 [DOI: 10.1109/36.581987]

Wang S P, Fang L, Gu X F, Yu T and Gao J. 2011. Comparison of aerosol optical properties from Beijing and Kanpur. Atmospheric Environment, 45(39): 7406−7414 [DOI: 10.1016/j.atmosenv.2011.06.055]

Waquet F, Goloub P, Deuzé J L, Léon J F, Auriol F, Verwaerde C, Balois J Y and François P. 2007. Aerosol retrieval over land using a multiband polarimeter and comparison with path radiance method. Journal of Geophysical Research, 112: D11214 [DOI: 10.1029/ 2006JD008029]

Xie Y, Zhang Y, Xiong X, Qu J J and Che H Z. 2011. Validation of MODIS aerosol optical depth product over China using CARSNET measurements. Atmospheric Environment, 45(33): 5970−5978 [DOI: 10.1016/j.atmosenv.2011.08.002]

# 北京地区 HJ-1 卫星 CCD 数据的气溶胶反演及在大气校正中的应用

方莉[1]，余涛[1]，顾行发[1]，王舒鹏[1]，高军[2]，刘其悦[1]

1. 遥感科学国家重点实验室 中国科学院遥感与数字地球研究所，北京 100101；
2. 国家国防科学技术工业局，北京 100037

**摘 要：**与现有的大气卫星传感器相比，环境一号卫星(HJ-1)CCD 相机具有较高的空间分辨率(30 m)，使得在城市地区找到光谱纯像元的机率大大增加。本文提出一种基于纯像元提取的城市地区气溶胶光学厚度(Aerosol Optical Depth，AOD)反演算法，利用像元纯净指数来提取 CCD 影像上的纯像元，并由 HJ-1 A 星和 B 星的多时相 CCD 观测数据结合地表双向反射率模型确定纯像元的地表反射特性，在此基础上反演 AOD。与 AERONET 地基测量数据的对比表明，该算法具有较高精度，相关系数为 0.83，线性拟合斜率为 1.091，截距为 0.053。基于该方法的 AOD 反演结果作为输入，能较大程度提高 HJ-1 卫星 CCD 影像大气校正的精度。

**关键词：**气溶胶光学厚度，气溶胶反演，环境一号卫星，大气校正，纯像元

**中图分类号：**TP79/P407.4 **文献标志码：**A

**引用格式：**方莉，余涛，顾行发，王舒鹏，高军，刘其悦．2013．北京地区 HJ–1 卫星 CCD 数据的气溶胶反演及在大气校正中的应用．遥感学报，17(1): 151–164

**Fang L, Yu T, Gu X F, Wang S P, Gao J, Liu Q Y. 2013. Aerosol retrieval and atmospheric correction of HJ-1 CCD data over Beijing. Journal of Remote Sensing, 17(1): 151–164**

## 1 引 言

遥感定量化的基础是机载或星载传感器的准确定标和遥感数据的大气纠正(Kaufman 和 Sendra，1988)。传感器获得的信号是地面信号和大气信号的叠加，大气影响不仅造成成像传感器图像模糊、对比度下降以及细节损失，还使后继的地表反射率、植被指数和叶绿素浓度等定量化反演结果严重偏离真值。大气校正的效果强烈依赖于输入的大气参数的精度，其中影响最大的是大气气溶胶参数(Fallah 等，1997；Liang 等，2001)。在校正过程中选用的气溶胶粒子光学厚度以及采用的模型对校正结果有很大的影响，因此精确探测气溶胶的消光特性及时空分布是遥感定量化中必不可少的重要环节。

由于卫星遥感手段具有高覆盖率、低重复周期和低成本等特点，它已成为探测全球气溶胶变化的重要手段(Kokhanovsky 和 Leeuw，2009)。根据数据源的不同，气溶胶反演方法可分为多波段方法(Kaufman 等，1997；Levy 等，2007)，多角度多波段方法(Peter 和 North，2002；Diner 等，2005)，及多角度偏振方法(Waquet 等，2007；Tanré 等，2011)。其中，有关 MODIS (Moderate-Resolution Imaging Spectro-radiometer)气溶胶反演方法的研究和应用广泛(Li 等，2007；Xie 等，2011)。MODIS 采用浓密植被法进行了气溶胶光学特性的反演，并于 2007 年对算法中的气溶胶模式和浓密植被在红外-可见光波段的地表反射率关系进行了改进(Levy 等，2007)。改进后的 C5 产品相对于原来 C4 产品，在中国地区的精度有了大幅度提升，但在部分城市地区的反演效果仍然不理想(Li 等，2007；Xie 等，2011)。可能的原因是红外-可见光波段地表反射率关

**收稿日期：**2011-12-26；**修订日期：**2012-03-12

**基金项目：**国家重点基础研究发展计划(973 计划)(编号：2010CB950803)

**第一作者简介：**方莉(1985— )，女，博士研究生，主要从事大气遥感研究。E-mail: lifang@irsa.ac.cn

**通信作者简介：**余涛(1967— )，男，博士，研究员，主要从事定量遥感研究。E-mail: yutao@irsa.ac.cn

系模型对于城市地区复杂下垫面不够精确(Oo 等，2010)。

目前用于气溶胶特性遥感的卫星传感器多为中低空间分辨率传感器，如 MODIS、MISR(Multi-angle Imaging Spectro Radiometer)和 POLDER(Polarization and Directionality of the Earth Reflectance)等。在城市地区，其成像像元多为混合像元，即每个像元都是由不同种类的地物目标组成的。此时制约气溶胶反演精度的一个重要因素即为混合像元的地表反射率特性估计与真实值的偏差。混合像元的地物组成比较复杂，很难对其反射特性进行精确的描述。因此，高精度的反演复杂下垫面条件下的气溶胶特性一直是气溶胶遥感的挑战之一。与混合像元相对应的是纯像元，其特点是包含一种占绝对主导的典型地物，其光谱一般是混合像元的最终端元。与混合像元相比，纯像元的地表反射特性相对稳定，其反射率特性可以通过地基观测或模型模拟来较高精度的刻画，因此针对纯像元上空的气溶胶特性进行反演，是解决复杂下垫面条件下的气溶胶特性反演的一种新途径。

与现有的大气卫星传感器相比，HJ-1 卫星 CCD 相机具有 30 m 的较高空间分辨率，在影像上特别是下垫面比较复杂的城市地区能找到纯像元的机率大大增加。本文基于 HJ-1 卫星 CCD 相机的高空间分辨率特性，提出一种通过光谱纯像元提取，反演城市地区复杂下垫面条件下的气溶胶光学厚度的方法，并依据该方法得到的 AOD 反演结果作为大气校正的参数，用于改善大气校正精度。

# 2 纯像元提取的城市地区气溶胶特性反演算法

## 2.1 辐射传输模拟方法

星载光学传感器接收到的表观辐射主要来自：遥感器视场内的大气分子、气溶胶粒子等散射太阳辐射的信息，通常称为程辐射；地表反射太阳光后直接进入传感器的辐射信息；来自传感器视场周围环境的辐射信息。大气层顶表观反射率 $\rho_\lambda^*(\theta_0,\ \theta,\ \phi)$ 可近似表达为(Vermote 等，1997；Levy 等，2007)：

$$\rho_\lambda^*(\theta_0,\theta,\phi)=\rho_\lambda^{\mathrm{a}}(\theta_0,\theta,\phi)+\frac{\rho_\lambda^{\mathrm{s}}}{1-\rho_\lambda^{\mathrm{s}}\cdot S_\lambda}\cdot T_\lambda(\theta_0)\cdot T_\lambda(\theta) \qquad (1)$$

式中，$\theta_0$、$\theta$ 和 $\phi$ 分别为太阳天顶角、传感器观测天顶角与传感器与太阳的相对方位角，$\lambda$ 为观测波长。上式右边第一项 $\rho_\lambda^{\mathrm{a}}$ 为大气程辐射项；第二项为地表和大气的共同贡献项，$S_\lambda$ 为大气半球反射率，$\rho_\lambda^{\mathrm{s}}$ 为地表双向反射率，$T_\lambda(\theta_0)$与 $T_\lambda(\theta)$分别为大气下行与上行辐射总透过率。上式中 $\rho_\lambda^{\mathrm{a}}$、$S_\lambda$，以及 $T_\lambda(\theta_0)\cdot T_\lambda(\theta)$均为气溶胶光学厚度 $\tau$ 的函数，遥感反演通常基于这一关系建立查找表来反演正确的气溶胶光学厚度。

## 2.2 纯像元的提取方法

本文基于像元纯度指数 PPI(Pixel Purity Index)来提取影像上的纯像元。PPI 是在高光谱数据中寻找“光谱最纯”像元的方法。传感器测量的光谱辐射值是非负的，由这些离散的辐射光谱构成的向量位于多维空间中，在该空间中形成一个凸的多维区域。凸多维区域的边界对应于纯像元(混合模型的最终光谱单元)，其他位于内部的向量可以认为是由这些边界单元线性混合而成。具体做法是，将 $N$ 维散点图重复投影到单位随机向量上，找出每次投影的极值像元，并对这些极值像元累计计数，产生一个像元纯度指数图，图中像元的值代表该像元在投影过程中为极值的次数。纯像元就是像元纯度指数图中数值较大的那些像元(Boardman 等，1993)。该方法被成功用于提取多光谱影像上的纯像元(胡姝婧 等，2010)。

## 2.3 算法介绍

HJ-1 卫星 CCD 相机的时间分辨率较高(2d)，使得收集相同纯像元不同方向的观测值的可能大大增加。这些观测值包含了晴朗天气以及污染天气的观测数据。对于高反射率地区的气溶胶光学厚度反演，如干旱半干旱地区(沙漠等)和城市地区等，许多研究假设在一定时间段内地表反射特性变化较小，基于该时间段内的清晰影像获取地表反射率来支持其他污染天气的 AOD 反演，包括深蓝算法(Hsu 等，2004)、结构函数法(Tanré 等，1988)以及 Liang 等人(2006)提出的针对亮地表地区的 MODIS 改进算法。该时间段通常为 3 个月 (Liang 等，2006)，如果有足够的晴空观测数据可考虑将时段设定为 1 个月(Hsu 等，2004)。但是该假设对于城市地区的混合像元存在较大的不确定性，一方面由于城市地区混合像元的地表反射率特性易受到人为活动的影响；另一方面，随着成像几何的变化，高大建筑物之间的遮挡造成的阴影使其反射率特性更加难以确定。本研究在使用 PPI 提取纯像元时，得到稳定存在的纯像元通常位于大块均匀地物目标的中心

处，受到人为活动影响较小，又能够较好地避免高大建筑物之间遮挡造成的阴影的影响，同时一定程度上降低了使用方向反射率分布 BRDF 模型刻画混合像元时引入的不确定性。算法的主要流程如下：

(1)根据辐射传输模型建立查找表：分析研究区域的气溶胶模式，在典型的气溶胶光学厚度下，基于辐射传输模式 6S(Vermote 等，1997)建立查找表。

(2)计算表观反射率，并依据云检测算法剔除有云的像元。

(3)选取一定时间段内的多幅晴朗天气影像，依据像元纯度指数提取纯像元，生成纯像元掩膜。城市地区受人类活动影响较大，纯像元目标在不同日期的影像上可能会发生变化，因此我们对多幅晴朗天气影像提取的纯像元进行筛选，保留该时间段内始终稳定存在的纯像元。

(4)依据晴朗天气观测值和 BRDF 模型确定纯像元 BRDF，并由此获取污染观测的纯像元地表反射率。本研究中使用 Roujean 地表 BRDF 模型 (Roujean 等, 1992)，拟合同一像元的模型参数需要至少 3 个观测值数据，即步骤(3)中至少选取 3 幅晴朗天气影像。对晴朗观测进行大气校正，得到特定成像几何下的纯像元地表反射率。通过 BRDF 模型融合多组成像几何下的地表方向反射率，确定模型参数，得到这一时期该像元的方向反射率分布。该像元污染天气下对应的地表反射率可以结合实际的成像几何得到。

(5)基于辐射传输查找表反演污染天气纯像元的气溶胶光学厚度。与地表特征相比，气溶胶光学厚度的空间变化比较平滑(Liang 等，2006)。在纯像元分布均匀的条件下，通过对整幅影像进行线性插值，得到逐像元的气溶胶光学厚度图。

### 2.4　验证与分析

根据已有研究(Wang 等，2011)，北京地区的气溶胶模式为粗细混合型，且以细粒子城市污染物为主，春季受沙尘粒子影响较大，月均气溶胶光学厚度变化范围是 0.5—1.8。根据地基气溶胶观测网 AERONET (Holben 等，1998)北京站点的观测数据，2009 年 8 月—10 月，北京气溶胶模式仍为粗细混合型，粗细粒子体积比约为 1.37。为了评估新算法的性能，使用 2009 年 8 月—10 月约 3 个月的数据反演了北京地区的气溶胶 AOD。反演结果与 AERONET 地基观测数据进行了比较验证。同时开展了过境时间相接近的 MODIS 气溶胶产品与 AERONET 数据的对比验证。为保证一致性，卫星反演的气溶胶光学厚度和地基测量值都为 550 nm 波段的结果。

根据卫星过境时 AERONET 北京站点的地基气溶胶测量值，选取 500 nm AOD 小于 0.1 的值作为北京的清洁大气状况(北京 2005 年—2009 年的 500 nm AOD 年平均值为 0.86)。图 1 显示了 CCD 相机红、绿、蓝波段真彩色合成影像上 AERONET 站点(39.977 °N, 116.381°E)在研究区域的位置及周围的纯像元分布示意图。

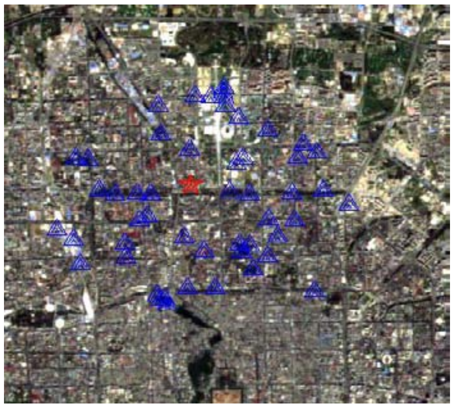

图 1　研究区 AERONET 北京站点位置(红色五角星)及周围纯像元(蓝色三角)分布图

设置一个固定的大气能见度，如 100 km(Liang 等，2006)，对晴朗天气影像进行大气校正。图 2 给出通过 Roujean 地表 BRDF 模型得到的典型纯像元(水泥：40.000 °N，116.382°E；植被：39.974°N，116.391°E)的蓝光波段 BRDF 模拟结果。

HJ-1 卫星观测 AOD 反演结果与 AERONET 地基测量数据的对比验证结果见图 3。验证中使用了与 HJ-1 卫星过境时间最接近的 AERONET 2 级直射光测量结果。地基数据与卫星数据的时间相差须小于 30 min，以保证地基观测与卫星过境之间大气状况的稳定。从图 3 可知，利用纯像元方法基于 HJ-1 卫星观测数据反演得到的大气气溶胶光学厚度与地基观测结果具有很好的一致性，二者相关系数为 0.83，线性拟合斜率为 1.091，截距为 0.053，均方根误差 RMSE 为 0.15。

图 3 同时给出了与 HJ-1 卫星过境时间接近的 MODIS 气溶胶产品与 AERONET 数据的对比验证结果。除 2009-10-15 地基测量与 MODIS 卫星过境时间间隔为 35 min 外，其余验证点的时间差均在 30 min 以

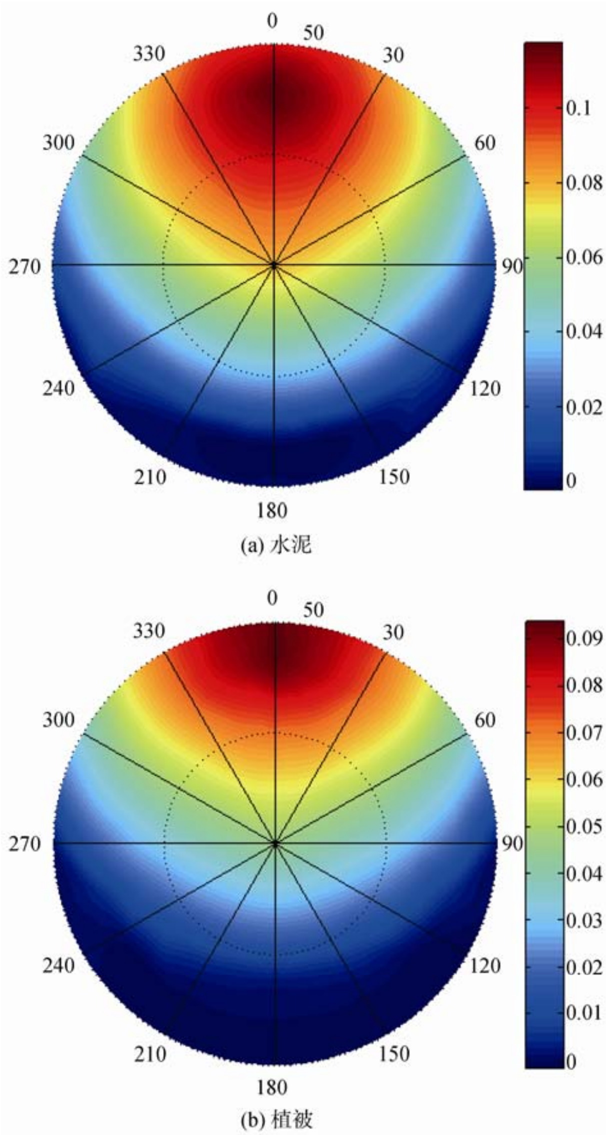


图 2　蓝光波段纯像元 BRDF 模拟结果

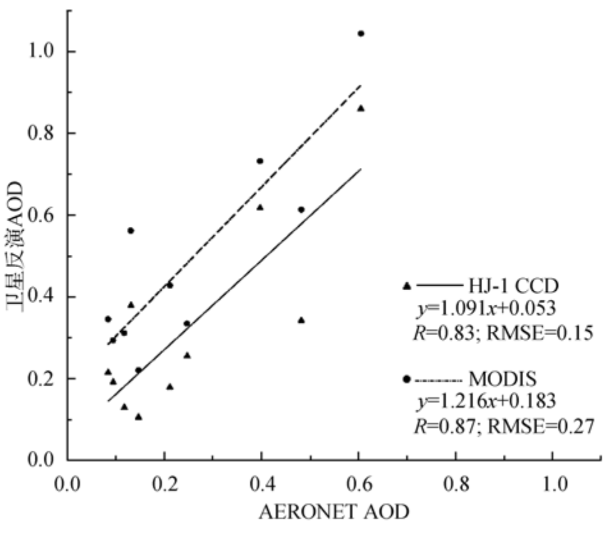


图 3　纯像元法反演的 CCD AOD 及 MODIS AOD 产品与 AERONET 测量值对比验证结果

内。图中二者线性拟合的斜率、截距及相关系数分别为 1.216、0.183 和 0.87，RMSE 为 0.27。从图 3 可以看出，CCD 反演 AOD 的线性拟合斜率与截距均优于 MODIS AOD，RMSE 也较小，但是相关系数 $R^2$ 略低。表 1 列出了所有验证数据的日期、卫星反演和 AERONET 地基测量结果，以及两组卫星反演值相对于地基测量的相对误差。数据显示，本次验证样本集以 AERONET 测量为基准，利用纯像元方法基于 HJ-1 观测值反演得到的 AOD 误差基本都小于 MODIS 的反演误差，整体精度有所提高，平均误差分别为 49%和 139%。Remer 等人(2005)定义陆地上高精度反演的误差阈值为 $0.05+0.15\tau_{\text{AERONET}}$。表 1 显示，HJ-1 和 MODIS 的多处反演结果误差大于该阈值。一方面是由于在城市地区即使通过纯像元的提取，精确地获得成像时刻的地表方向反射率仍然比较困难；另一方面是由于选用验证数据集的气溶胶光学厚度值偏低(样本均值仅为 0.25)，在地气耦合系统中大气贡献相对较小，使得卫星观测值对气溶胶光学特性的敏感度降低(Bréon 等，2011)。从总体结果来看，利用纯像元方法，HJ-1 卫星 CCD 数据是可以有效的用于城区气溶胶监测，为高精度的大气校正提供输入参数的。

## 3　基于辐射传输模型的大气校正

为精确得到下垫面的方向反射特性，纯像元法反演得到的气溶胶 AOD，采用基于辐射传输模型的大气校正方法对 HJ-1 卫星 CCD 影像进行逐像元地表反射率反演。图 4 和图 5 分别为 2009-08-13 覆盖北京市城区及其周边地区影像第 1 波段(蓝光)和第 3 波段(红光)校正前后反射率图。

校正前后的反射辐射亮度和图像对比度有明显的变化。大气校正前，地物受到大气吸收和散射的影响模糊不清，对比度不高。大气校正后，有效地消除了气溶胶和水汽、臭氧等气体的影响，恢复了地物目标的原貌，图像对比度提高。而且，由于短波波段受大气分子散射和气溶胶散射影响更大，图中可见短波(第 1 波段)校正前后影像差别较大。而红光波段受其影响相对较小，校正前后差别较小。

为了定量评价大气校正的精度，将校正前后的地表反射率与实测地表反射率进行比较，同时也给出了利用基于图像特征的暗像元方法(Kaufman, 1989)进行大气校正的结果。图 6 为 2009-08-13 CCD 影像上验

表 1 HJ-1 CCD、MODIS 和 AERONET 的 AOD 结果及相对误差

| 日期 | HJ-1 AOD | MODIS AOD | AERONET AOD | HJ-1 与 AERONET AOD 相对误差/% | MODIS 与 AERONET AOD 相对误差/% |
|---|---|---|---|---|---|
| 2009-08-02 | 0.3792 | 0.5620 | 0.1311 | 189 | 329 |
| 2009-08-13 | 0.6172 | 0.7320 | 0.3969 | 56 | 84 |
| 2009-08-23 | 0.3426 | 0.6130 | 0.4817 | –29 | 27 |
| 2009-09-21 | 0.1300 | 0.3120 | 0.1175 | 11 | 166 |
| 2009-10-02 | 0.2153 | 0.3460 | 0.0842 | 156 | 311 |
| 2009-10-05 | 0.1794 | 0.4280 | 0.2113 | –15 | 103 |
| 2009-10-09 | 0.8600 | 1.0440 | 0.6044 | 42 | 73 |
| 2009-10-14 | 0.1920 | 0.2940 | 0.0945 | 103 | 211 |
| 2009-10-15 | 0.2559 | 0.3350 | 0.2468 | 4 | 36 |
| 2009-10-17 | 0.1061 | 0.2210 | 0.1467 | –28 | 51 |
| **平均值** | **0.3278** | **0.4887** | **0.2515** | **49** | **139** |

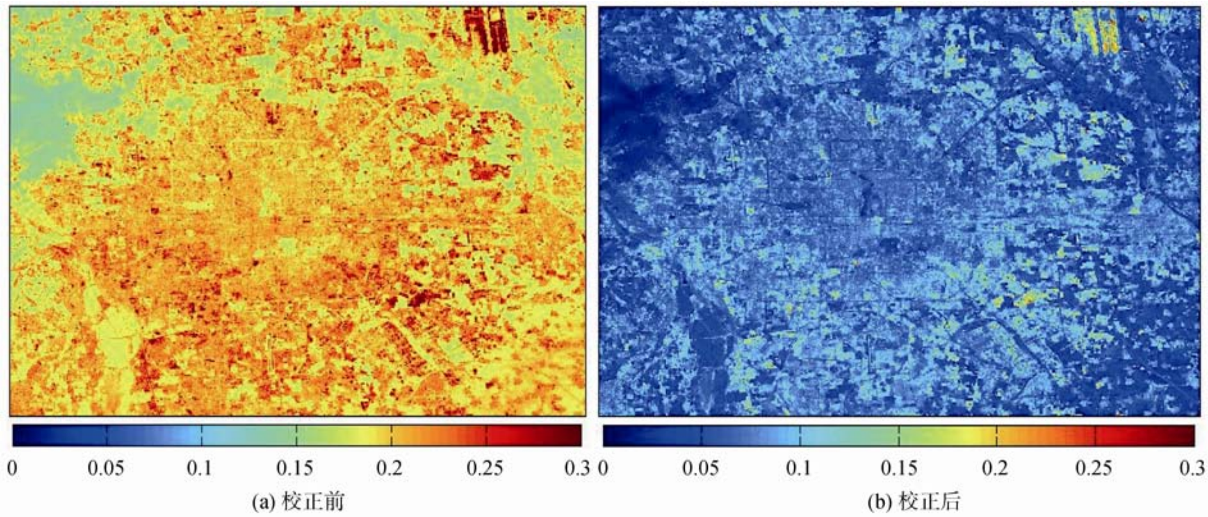


图 4 第 1 波段校正前、后反射率影像

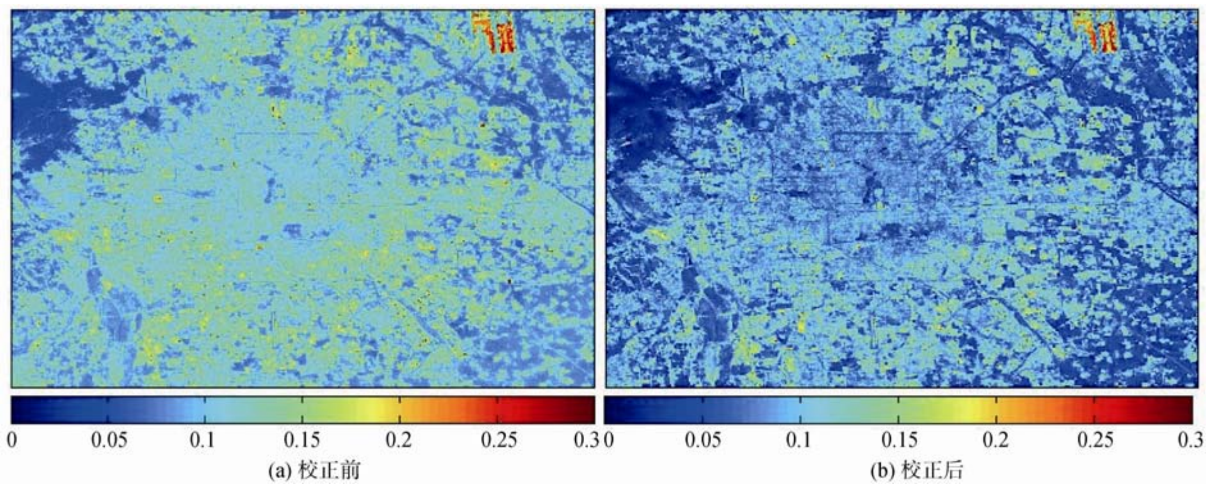


图 5 第 3 波段校正前、后反射率影像

证点位置示意图(水泥：39.993°N，116.393°E；植被：39.991°N，116.434°E)。

验证结果(图 7)显示，校正后的地表反射率相比校正前有较大变化，校正后的地表反射率更接近实测的真实值，较好地纠正了由于大气散射和吸收对卫星观测数据造成的影响。而同暗像元方法相比，本方法更

接近地表实测反射率，校正精度大幅度提高。

图 6　大气校正验证点位置示意图
(红色：水泥路面；绿色：植被)

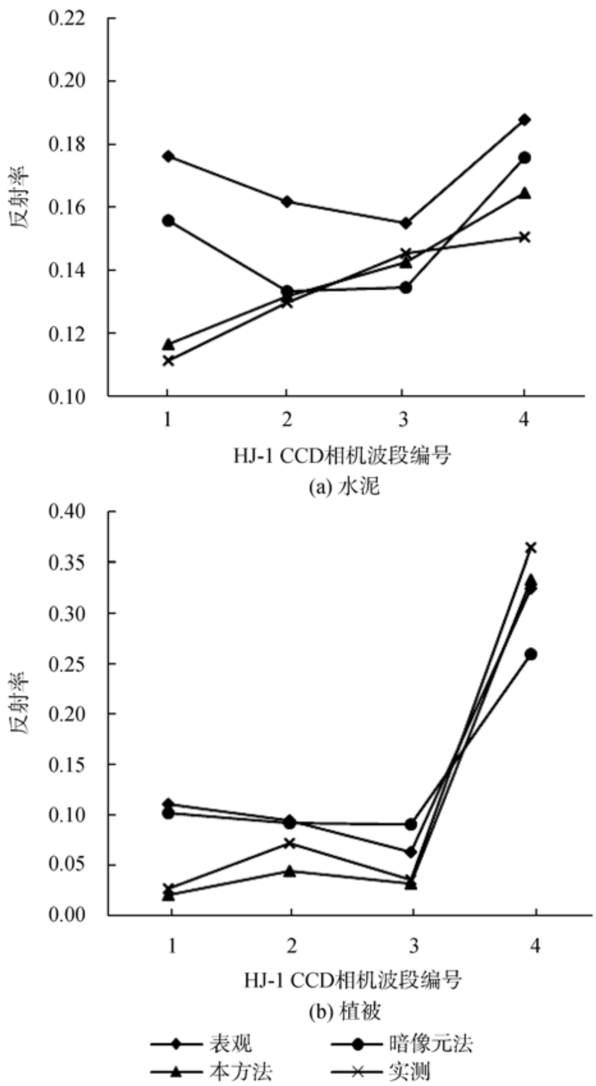


图 7　水泥和植被大气校正前后反射率及与地面实测反射率对比

# 4　结　论

本文提出了基于光谱纯像元由 HJ-1 卫星 CCD 数据反演城市地区大气气溶胶光学厚度的方法，并以北京地区 AERONET 站点的观测数据对反演的结果进行验证，结果显示，本算法具有较高的反演精度(二者相关系数为 0.83，线性拟合斜率为 1.091，截距为 0.053，均方根误差为 0.15)。与近似同一时刻 MODIS 的 AOD 产品进行对比，初步证明本文反演方法的有效性。基于本算法得到的 AOD 反演结果作为输入，采用辐射传输模型法对 HJ-1 卫星在北京地区的 CCD 影像进行了大气校正。校正前后的图像视觉效果及定量的与地面实测反射率的比较结果，都显示了该方法的大气校正具有较高的精度，能够为 HJ-1 卫星数据的定量化应用奠定基础。该算法的稳定性和精度评价需要针对更大范围的区域和更大的时间跨度开展进一步的验证分析及相关研究。

## 参考文献(References)

Boardman J W, Kruse F A and Green R O. 1993. Automating spectral unmixing of AV I R IS data using convex geometry concepts // Summaries, Forth Annual JPL Airborne Geoscience Workshop. Pasadena, CA, US: JPL Publication, 26(1): 11–14

Bréon F M, Vermeulen A and Descloitres J. 2011. An evaluation of satellite aerosol products against sunphotometer measurements. Remote Sensing Environment, 115(12): 3102–3111 [DOI: 10.1016/j.rse.2011.06.017]

Diner D J, Martonchik J V, Kahn R A, Pinty B, Gobron N, Nelson D L and Holben B N. 2005. Using angular and spectral shape similarity constraints to improve MISR aerosol and surface retrievals over land. Remote Sensing of Environment, 94(2): 155–171

Fallah A, Jaja J, Liang S, Kaufman Y J and Townshend J R G. 1997. Fast algorithms for atmospheric correction from Landsat TM over land. Journal of Geophysical Research, 102: 17173–17186

Holben B N, Eck T F, Slutsker I, Tanré D, Buis J P, Setzer A, Vermote E, Reagan J A, Kaufman Y J, Nakajima T, Lavenu F, Jankowlak I and Smirnov A. 1998. AERONET-A federated instrument network and data archive for aerosol characterization. Remote Sensing of Environment, 66(1): 1–16 [DOI: 10.1016/S0034-4257(98)00031-5]

Hsu N C, Tsay S C, King M D and Herman J R. 2004. Aerosol properties over bright-reflecting source regions. IEEE Transacitons on Geoscience and Remote Sensing, 42(3): 557–569 [DOI: 10.1109/TGRS.2004.824067]

胡姝婧，胡德勇，赵文吉. 2010. 基于 LSMM 和改进的 FCM 提取城市植被覆盖度-以北京市海淀区为例. 生态学报，30(4): 1018–1024

Kaufman Y J. 1989. The atmospheric effect on remote sensing and its correction // Asrar G, ed. Theory and Application of Optical Remote Sensing, New York: Wiley: 341

Kaufman Y J and Sendra C. 1988. Algorithm for automatic atmospheric corrections to visible and near-IR satellite imagery. International Journal of Remote Sensing, 9(8): 1357–1381 [DOI: 10.1080/01431168808954942]

Kaufman Y J, Tanré D, Remer L A, Vermote E F, Chu A and Holben B N. 1997. Operational remote sensing of tropospheric aerosol over land from EOS moderate resolution imaging spectroradiometer. Journal of Geophysical Research, 102(D14): 17051–17067 [DOI: 10.1029/96JD03988]

Kokhanovsky A A and Leeuw G. 2009. Satellite Aerosol Remote Sensing Over Land. UK: Praxis Publishing Ltd, Chichester

Levy R C, Remer L A, Mattoo S, Vermote E F and Kaufman Y J. 2007. Second-generation operational algorithm: retrieval of aerosol properties over land from inversion of Moderate Resolution Imaging Spectroradiometer spectral reflectance. Journal of Geophysical Research, 112: D13211 [DOI: 10.1029/2006JD007811]

Li Z Q, Niu F, Lee K H, Xin J Y, Hao W M, Nordgren B L, Wang Y S and Wang P C. 2007. Validation and understanding of Moderate Resolution Imaging Spectroradiometer aerosol products (C5) using ground-based measurements from the handheld Sun photometer network in China. Journal of Geophysical Research, 112: D22S07 [DOI: 10.1029/2007JD008479]

Liang S, Fang H and Chen M. 2001. Atmospheric correction of landsat ETM+ land surface imagery: I. Methods. IEEE Transactions on Geoscience and Remote Sensing, 39(11): 2490–2498 [DOI: 10.1109/36.964986]

Liang S L, Zhong B and Fang H L. 2006. Improved estimation of aerosol optical depth from MODIS imagery over land surfaces. Remote Sensing of Environment, 104(4): 416–425 [DOI: 10.1016/j.rse.2006.05.016]

Oo M M, Jerg M, Hernandez E, Picon A, Gross B M, Moshary F and Ahmed S A. 2010. Improved MODIS aerosol retrieval using modified VIS/SWIR surface albedo ratio over Urban Scenes. IEEE Transactions on Geoscience and Remote Sensing, 48(3): 983–1000 [DOI: 10.1109/TGRS.2009.2028333]

Peter R and North J. 2002. Estimation of aerosol opacity and land surface bidirectional reflectance from ATSR-2 dual-angle imagery: operational method and validation. Journal of Geophysical Research (Atmos), 107: 4149 [DOI: 10.1029/ 2000JD0-00207]

Remer L A, Kaufman Y J, Tanré D, Mattoo S, Chu D A, Martins J V, Li R R, Ichoku C, Levy R C, Kleidman R G, Eck T F, Vermote E, and Holben B N. 2005. The MODIS Aerosol algorithm, products, and validation. Journal of the Atmospheric Sciences, 62(4), 947–973 [doi: 10.1175/JAS3385.1]

Roujean J L, Leroy M and Deschamps P Y. 1992. A bidirectional reflectance model of the Earth's surface for the correction of remote sensing data. Journal of Geophysical Research, 97(D18): 20455–20468 [DOI: 10.1029/92JD01411]

Tanré D, Bréon F M, Deuzé J L, Dubovik O, Ducos F, Francois P, Goloub P, Herman M, Lifermann A and Waquet F. 2011. Remote sensing of aerosols by using polarized, directional and spectral measurements within the A-Train: the PARASOL mission. Atmospheric Measurement Techniques Discussions, 4(2): 2037–2069 [DOI: 10.5194/amtd-4-2037-2011]

Tanré D, Deschamps P Y, Devaux C and Herman M. 1988. Estimation of Saharan aerosol optical thickness from blurring effects in thematic mapper data. Journal of Geophysical Research, 93(D12): 15955–15964 [DOI: 10.1029/JD093iD12p15955]

Vermote E F, Tanré D, Deuzé J L, Herman M and Morcette J J. 1997. Second simulation of the satellite signal in the solar spectrum, 6S: an overview. IEEE Transactions on Geoscience and Remote Sensing, 35(3): 675–686 [DOI: 10.1109/36.581987]

Wang S P, Fang L, Gu X F, Yu T and Gao J. 2011. Comparison of aerosol optical properties from Beijing and Kanpur. Atmospheric Environment, 45(39): 7406–7414 [DOI: 10.1016/j.atmosenv.2011.06.055]

Waquet F, Goloub P, Deuzé J L, Léon J F, Auriol F, Verwaerde C, Balois J Y and François P. 2007. Aerosol retrieval over land using a multiband polarimeter and comparison with path radiance method. Journal of Geophysical Research, 112: D11214 [DOI: 10.1029/2006JD008029]

Xie Y, Zhang Y, Xiong X, Qu J J and Che H Z. 2011. Validation of MODIS aerosol optical depth product over China using CARSNET measurements. Atmospheric Environment, 45(33): 5970–5978 [DOI: 10.1016/j.atmosenv.2011.08.002]